

Timing of Z-ring localization in *Escherichia coli*

This article has been downloaded from IOPscience. Please scroll down to see the full text article.

2011 Phys. Biol. 8 066003

(<http://iopscience.iop.org/1478-3975/8/6/066003>)

View [the table of contents for this issue](#), or go to the [journal homepage](#) for more

Download details:

IP Address: 132.72.87.32

The article was downloaded on 21/11/2011 at 16:42

Please note that [terms and conditions apply](#).

Timing of Z-ring localization in *Escherichia coli*

R Tsukanov^{1,2}, G Reshes^{1,2,3}, G Carmon^{1,2}, E Fischer-Friedrich⁴,
N S Gov⁴, I Fishov⁵ and M Feingold^{1,2,6}

¹ Department of Physics, Ben-Gurion University of the Negev, Beer-Sheva 84105, Israel

² The Ilse Katz Center for Nanotechnology, Ben-Gurion University of the Negev, Beer-Sheva 84105, Israel

³ Sami Shamoon College of Engineering, Beer-Sheva 84100, Israel

⁴ Department of Chemical Physics, Weizmann Institute of Science, Rehovot 76100, Israel

⁵ Department of Life Sciences, Ben-Gurion University of the Negev, Beer-Sheva 84105, Israel

E-mail: mario@bgu.ac.il

Received 28 July 2011

Accepted for publication 13 September 2011

Published 21 October 2011

Online at stacks.iop.org/PhysBio/8/066003

Abstract

Bacterial cell division takes place in three phases: Z-ring formation at midcell, followed by divisome assembly and building of the septum per se. Using time-lapse microscopy of live bacteria and a high-precision cell edge detection method, we have previously found the true time for the onset of septation, τ_c , and the time between consecutive divisions, τ_g . Here, we combine the above method with measuring the dynamics of the FtsZ-GFP distribution in individual *Escherichia coli* cells to determine the Z-ring positioning time, τ_z . To analyze the FtsZ-GFP distribution along the cell, we used the integral fluorescence profile (IFP), which was obtained by integrating the fluorescence intensity across the cell width. We showed that the IFP may be approximated by an exponential peak and followed the peak evolution throughout the cell cycle, to find a quantitative criterion for the positioning of the Z-ring and hence the value of τ_z . We defined τ_z as the transition from oscillatory to stable behavior of the mean IFP position. This criterion was corroborated by comparison of the experimental results to a theoretical model for the FtsZ dynamics, driven by Min oscillations. We found that $\tau_z < \tau_c$ for all the cells that were analyzed. Moreover, our data suggested that τ_z is independent of τ_c , τ_g and the cell length at birth, L_0 . These results are consistent with the current understanding of the Z-ring positioning and cell septation processes.

 Online supplementary data available from stacks.iop.org/PhysBio/8/066003/mmedia

1. Introduction

The divisome is a super-complex that drives bacterial cytokinesis [1–4]. It consists of an annular core, the Z-ring and an associated family of proteins encoded by the filamentous temperature-sensitive (fts) genes [5–8]. The formation of the divisome is tightly controlled in both space and time [9–11]. It was shown that in *Escherichia coli*, for example, the divisome is located at mid-cell with remarkable accuracy, $\sim 4\%$ [12]. This accuracy may be attributed to the combined effect of two independent mechanisms, namely MinCDE oscillations

[13, 14] and nucleoid occlusion [15, 16]. The Min system consists of the MinC, MinD and MinE proteins. MinC inhibits the polymerization of FtsZ, MinD recruits MinC to the cytoplasmic membrane and MinE drives MinC-MinD off the cytoplasmic membrane. As a result, the MinC-MinD complex oscillates between cell caps and is mostly absent in the vicinity of the cell center [17–25]. The second mechanism, the nucleoid occlusion mechanism, is believed to inhibit the formation of the Z-ring in the vicinity of the nucleoid. It has been shown that the inhibitory action of the nucleoid is mediated by Noc (YyaA) in *Bacillus subtilis* [26] and by SlmA in *E. coli* [27].

⁶ Author to whom any correspondence should be addressed.

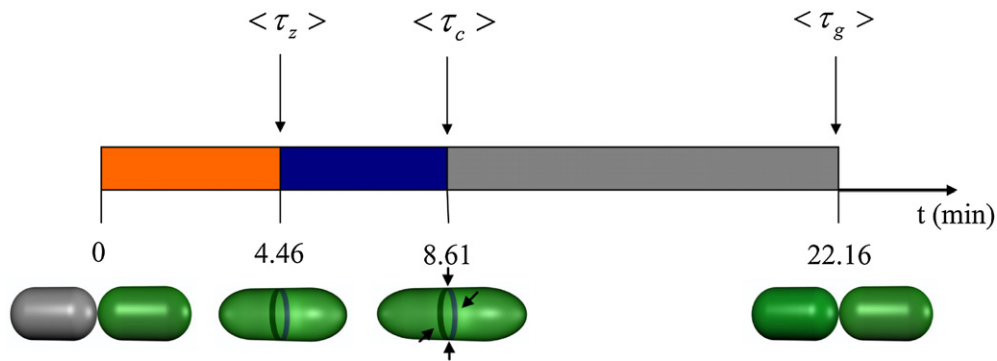


Figure 1. Schematic representation of the sequence of events: cell birth, Z-ring positioning, onset of septation and end of cell division. The different time intervals are color coded as follows: orange—the period from cell birth to Z-ring positioning, τ_z ; dark blue—the period from τ_z to the onset of septation, τ_c ; gray—the T-period.

In the time domain, Z-ring formation represents the first event of the division process. It takes place via the condensation of FtsZ oligomers. Several possible scenarios describing this process have been proposed [28–32]. For some time, it was believed that the FtsZ oligomers condense directly from the cytoplasm. More recently, however, helical FtsZ structures were observed on the cytoplasmic membrane along with Z-ring formation [33]. This finding led to the suggestion that FtsZ forms helices on the cytoplasmic membrane that later condense into a ring [34]. Three assisting proteins are involved at an early stage in Z-ring formation, FtsA and ZipA anchor FtsZ to the membrane and the ring-stabilizing ZapA protein localizes at midcell together with FtsZ. Subsequently, ten other proteins adhere to the ring: FtsE, FtsX, FtsK, FtsQ, FtsL, FtsB, FtsW, FtsI, FtsN and AmiC [5–8]. Although these proteins localize in an apparently sequential fashion, it was found that some of them associate before joining the divisome [35, 36, 7]. Moreover, it was proposed that the divisome is assembled in two steps [37]. The first, which occurs immediately after Z-ring formation, involves the first half of the divisome proteins, presumably ending with FtsK. In the second step, which is delayed by a time interval that was found to vary between 14 and 21 min for the *E. coli* strains and the growth conditions used in [37], FtsK, FtsQ, FtsL, FtsB, FtsW, FtsI, FtsN and AmiC bind to the Z-ring, thereby completing the formation of the divisome. Following divisome maturation, constriction of the cell envelope can begin. It is presently not clear whether septation starts immediately upon divisome maturation or, alternatively, whether it requires an additional signal. Such a signal may, for example, originate from a certain stage in chromosome segregation.

Although the sequence of events during bacterial cytokinesis has been established, the timing is known only partially. den Blaauwen *et al* and Aarsman *et al* [38, 37] used a statistical approach to obtain the average times at which the various division events occur. Specifically, the cell length distribution of asynchronous populations was translated into the corresponding age distributions for the appearance of a particular feature, e.g. the Z-ring. In fact, the resulting age distributions were analyzed only with the aim of extracting their averages. The statistical approach for determining the timing of events is, however, limited in two important ways.

First, it cannot reveal the time correlations between different events in individual cells. Second, due to the lack of dynamical information, its ability to interpret the appearance of specific cellular structures is constrained. Both these shortcomings can be circumvented by using a dynamic single cell approach to determine the timing of cell cycle events [39, 40].

We have recently shown that measuring the dynamics of the septal width for individual cells with high accuracy facilitates determination of the time at which envelope constriction begins, τ_c , and the time between consecutive divisions, τ_g (figure 1) [39, 40]. In what follows, we refer to τ_g as the generation time. We found that, on average, τ_c occurs about 5 min before the visible constriction, τ_{cv} , for cells with a 24 min generation time. The large difference between τ_c and τ_{cv} is due to the combined effect of two factors. The first is the limited resolution of the optical microscope, which does not allow the observation of the constriction in its initial stages. The second factor is the extremely slow rate of constriction for times close to τ_c . Specifically, we have found that at the end of the first quarter of the division time, $\tau_g - \tau_c$ (the T-period), the constriction reaches only about 97% of the cell width. Moreover, using single cell values of τ_c and τ_g , we have shown that, for given strain and growth conditions, $\tau_c(\tau_g)$ is roughly linear and $\tau_g - \tau_c$ is independent of τ_g within experimental error [39, 40]. We have also found evidence for correlations between several other single-cell parameters.

Problems analogous to those that arise in measuring τ_c will also be manifested in timing other events of the bacterial cell cycle. In particular, the Z-ring positioning time, τ_z , is to some extent ambiguously defined. Previously, τ_z was identified with the appearance of an FtsZ structure around midcell and was determined by visual inspection [38]. Since in the single-cell approach we aim to establish the transition between a disperse FtsZ cloud and the newly formed Z-ring, a quantitative method for measuring τ_z is required.

To obtain an accurate description of the Z-ring dynamics, we used in this study the integral of the fluorescence intensity over the cell width, i.e. the integral fluorescence profile (IFP). The integration of the intensity reduces the noise level, thus improving the signal-to-noise ratio. An additional advantage of the IFP is that it enables analysis of the Z-ring in the presence of helical structures along the cytoplasmic membrane: since

the integration runs along the ring but only intersects the helix, it leads to a significant enhancement of the signal from the ring over the signal from the helix. The IFP was previously used by Guberman *et al* [41] to analyze the asymmetry of SpoIIE localization during *B. subtilis* sporulation and the accuracy of cell division in *E. coli*.

In this study, we used the IFP approach to monitor the dynamics of the FtsZ distribution over the entire cell cycle; we defined τ_z as the time at which the center of this distribution settled into the vicinity of its final position. We found that for all cells, $\tau_z < \tau_c$ and that τ_z was apparently not correlated with τ_c , τ_g or the cell length at birth, L_0 .

2. Materials and methods

2.1. Bacterial strain and growth conditions

E. coli strain EC448 was kindly supplied by Weiss [42]. This strain contains a chromosomal copy of *ftsZ-gfp* under the control of a modified *trc* promoter. Under moderate induction conditions, the fraction of FtsZ-GFP lies between 30% and 40% of the total FtsZ [33]. Although FtsZ-GFP is not fully functional, strain EC448 displayed normal growth and division behavior. In our experiments, cells were grown at 37° in Luria Broth (LB) until $OD_{600} \cong 0.2$ in the exponential regime. FtsZ-GFP expression was induced with 40 μM IPTG for the final 1.5 to 2 h of the culture. We confirmed that the presence of IPTG did not affect the behavior or the growth pattern of the cells.

In a series of four independent experiments, the results of which are presented below, the average generation time in liquid culture was $\langle \tau_{g,s} \rangle = 24.3 \pm 0.5$ ($\pm\text{SE}$) min. Each experiment allowed us to monitor under the microscope several individual cells growing on agar gel. (A description of the microscopy sample preparation procedure is presented in the next section.) A total of 15 individual cells were monitored and analyzed. To test whether the induced cells growing on agar displayed a normal division cycle, we measured τ_c and τ_g for each cell using the method described in [39]. First, we found that $\langle \tau_g \rangle = 22.2 \pm 0.8$ min, where $\langle \dots \rangle$ denotes the average over the 15 cells, i.e. a value only slightly shorter than $\langle \tau_{g,s} \rangle$. Moreover, an analysis of the dependence of τ_c on τ_g , $\tau_c(\tau_g)$, showed $\tau_c(\tau_g)$ to be linear within experimental error. The linearity of $\tau_c(\tau_g)$ is consistent with the behavior observed for cells that were grown without inducer [39, 40]. Therefore, in what follows, we assumed that the cell cycle is not affected by 40 μM IPTG.

Although Z-ring images of our cells showed typically good contrast, the level of noise was not negligible. Therefore, to obtain much higher signal-to-noise ratios, we performed a second type of experiment in which 500 μM IPTG was used for the induction of FtsZ-GFP expression. In what follows, we refer to 500 μM IPTG experiments as the high-induction type and to 40 μM IPTG experiments as the low-induction type. While the aim of the high-induction experiments was to obtain high-quality visualization of the Z-ring, that of the low-induction experiments was to time the localization of the Z-ring and to monitor the dynamics of the FtsZ distribution over the entire cell cycle.

In the high-induction experiments, the growth of the cells in the liquid medium did not appear to be affected by the addition of IPTG. On the other hand, on the solid substrate, cells exposed to IPTG appeared to grow normally only until the first division. Thereafter, cell growth was slower than that in the absence of the inducer, and a certain fraction of these cells did not reach the second division. Despite these cell cycle anomalies in the high-induction experiments, we found that the structure of the Z-ring was apparently the same as that in low-induction experiments but that in microscopy the contrast was far superior in the high-induction experiments.

2.2. Microscopy

Our imaging setup consisted of an inverted fluorescence microscope (IX70, Olympus) and a cooled intensified CCD camera (IPentamax, Princeton Instruments). We used a 100 \times objective (UPLFLN 100 \times 02 PH, oil immersion, $NA = 1.3$). The pixel size corresponded to 70 nm, and the depth of field was 0.34 μm [43]. Computer-controlled shutters (Uniblitz) blocked either the halogen or the mercury lamps. The shutters were synchronized with the camera and opened only during the exposure time. This approach reduced the photobleaching of GFP and the photodamage to cells. It also allowed us to alternate between phase-contrast and fluorescence frames in a time-lapse experiment. The temperature of the sample was maintained at 37° by heating the objective. The focus was adjusted manually throughout the experiment.

To monitor the dynamics of FtsZ-GFP in individual cells, 10 μl of bacterial culture was loaded onto a thin layer of 1.5% agar with LB (Sigma) and IPTG and covered with a cover slip. Cell dynamics was recorded for about two generations, i.e. we followed an isolated cell starting around its half cycle until it became a micro-colony of four separated cells. Each imaging cycle consisted of nine phase-contrast frames taken 4 s apart, followed by a fluorescence frame after 1 s. All frames had exposure times of 0.5 s such that the length of the imaging cycle was 42 s. While phase-contrast images were used to monitor cell morphogenesis, fluorescence frames were used to follow the changes in the FtsZ-GFP distribution. For establishing the timing of the sequence of events in cytokinesis, phase-contrast images are required to obtain τ_c and τ_g and fluorescence frames are needed to determine τ_z .

The structure of the imaging cycle described above was chosen in such a way as to reduce the bleaching of FtsZ-GFP on the timescale of the cell cycle. This requirement, however, limited the time resolution and hence resulted in some of the finer details of the Z-ring dynamics being missed. To improve the time resolution, we also performed experiments that had a shorter imaging cycle but extended over times significantly shorter than τ_g . We refer to such experiments as zoom type. They were performed only on high-induction cells. In zoom experiments, the imaging cycle consisted of only three frames—two phase-contrast frames followed by a fluorescence frame. The time between the first two frames was 1 s and that between the second and the third was 0.5 s. As before, exposure time was 0.5 s for all frames, such that the length of the imaging cycle was 4 s. To further improve

the signal-to-noise ratio, in zoom experiments we used 3% agarose gel instead of agar. The fluorescence data from zoom experiments were indeed significantly less noisy than those from regular high-induction experiments. This improvement is due to both the reduced bleaching during the shorter total exposure time and the lower background fluorescence of the agarose gel. However, the main advantage of the zoom experiments lay in the fact that, due to the relatively high density of the gel, the daughter cells continued to grow along the same axis as that of the mother cell (see figure 4), which facilitated a uniform description of the FtsZ distribution for both mother and daughter cells. Note that in these experiments we monitored only a fraction of the cell cycle and, as a result, we could not accurately time the observed events relative to the cycle.

2.3. Image analysis

Our method for obtaining τ_c and τ_g for a particular cell from a phase-contrast time-lapse movie of its cell cycle has been described in detail elsewhere [39]. Below, we explain the approach that we used for the analysis of the fluorescence images.

In our microscopy sample, *E. coli* cells are oriented with their long axis perpendicular to the optical axis, z . Correspondingly, the Z-ring is parallel to the z -axis, and its image appears as a broadened section of the true structure. This broadening is due to diffraction and is characterized by the three-dimensional point spread function (3D PSF) of the microscope. We described the fluorescence images of the Z-ring in terms of a 2D intensity distribution, $I(x, y)$, which, for $\tau_z < t < \tau_c$, resembled a strip with two intensity peaks located in the vicinity of the cytoplasmic membrane (see cell images in figure 4). As the cell starts to constrict, the two peaks gradually approach each other until they coalesce. Due to the relatively low expression level of FtsZ-GFP in the low-induction experiments and to the effects of bleaching, the measured $I(x, y)$ distributions were rather noisy. Thus to improve the signal-to-noise ratio, we further reduced the data by projecting $I(x, y)$ onto the long cell axis, u ; we refer to the result of this projection as the IFP.

To obtain the IFP, we first defined the cell axis, u , as the long axis of the best-fitting ellipse to the cell contour (figure 2). Next, starting from one of the end points of the u -axis, at intervals of 1 pixel from each other, we defined v -axes that are all perpendicular to the u -axis. IFP(u) was defined as a discrete and finite approximation of the integral of $I(x, y)$ along the v -axes, namely, we summed the values of the fluorescence intensity along each of the v -axes at intervals of 1 pixel up to the cell contour. In zoom experiments, in which daughter cells grew collinearly, we extended the integration range starting from a distance of 10 pixels on one side of the u -axis and ending at a distance of 10 pixels on the other. In general, the (x, y) positions of the terms in these sums did not correspond to the center of a particular pixel. We therefore approximated the values of $I(x, y)$ at these points by 2D linear interpolation [44]. For the interpolation, we assumed that the intensity values of pixels corresponded to the (x, y) point at

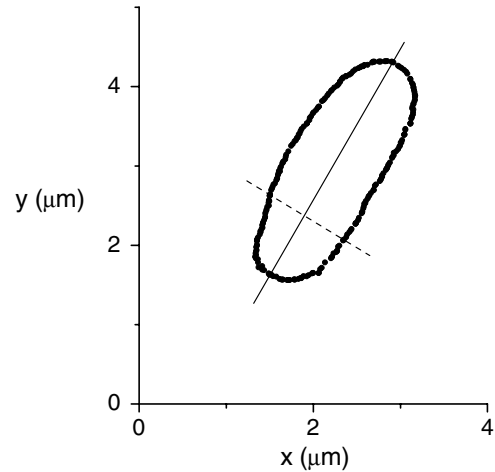


Figure 2. Illustration of the way in which the IFP is computed (see the text). The cell contour (squares) corresponds to the cell of figures 5 and 6 at $t = 8.47$ min. The long axis of the cell, u , is shown (solid line) together with one of the perpendicular axes, v (dashed line).

their center. Then, the value of $I(x, y)$ at an arbitrary point could be approximated by the plane defined by the centers of the three closest pixel centers.

3. Results

3.1. Structure of the Z-ring image

As discussed in section 2, the high-induction experiments produced images of FtsZ-GFP distributions with significantly better contrast than that in the low-induction experiments. Therefore, we used the output of the high-induction experiments for the analysis of the structure of FtsZ-GFP images and the corresponding IFPs.

In figure 3(a), we show the IFP for two Z-rings. The image was obtained from a zoom experiment and corresponds to two collinear daughter cells (see figure 4(c)). This configuration is optimal for a quantitative analysis of the IFP. In this case, there is no contribution from the septum between the cells, which allows us to identify the single Z-ring contribution to the IFP. Accordingly, in figures 3(b) and (c), we show the IFP data of figure 3(a) on half logarithmic plots. That is, in figure 3(b), we plot the IFP data to the left of the first peak as a function of the distance from this peak. Similarly, in figure 3(c) we plot the IFP data to the right of the second peak as a function of the distance from the peak. In both figures 3(b) and (c), we found good agreement with an exponential function. This behavior was common to all the IFPs, including those from the low-induction experiments. We therefore used a sum of exponential functions to describe the experimentally measured IFPs as follows:

$$f(u) = \sum_{i=1}^N A_i \exp(-|u - u_i|/k_i), \quad (1)$$

where N is the number of ring-like formations, and A_i , u_i and k_i are the corresponding amplitude, center and decay

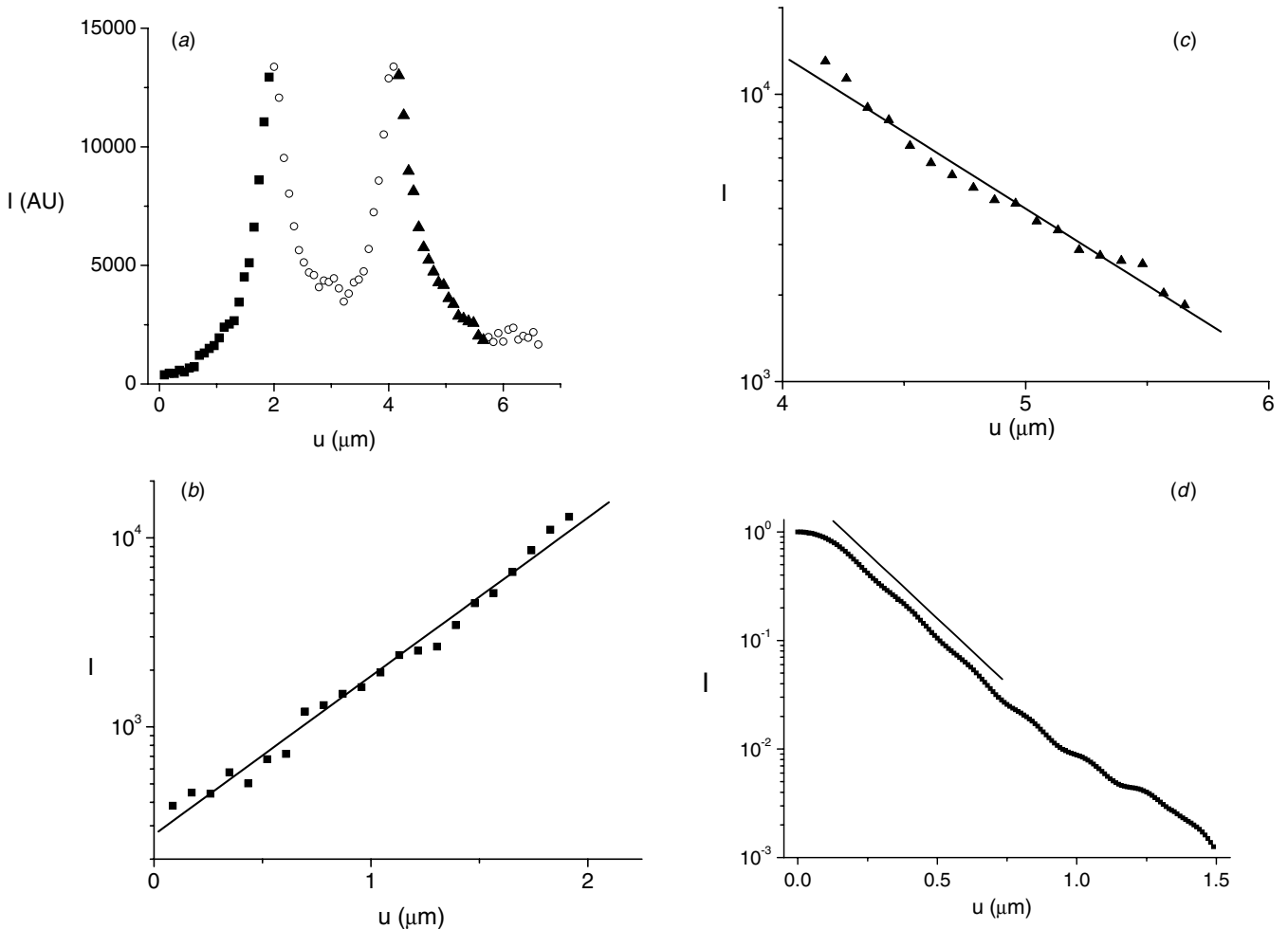


Figure 3. IFPs for two daughter cells growing collinearly (in a zoom experiment). (a) The different symbols distinguish between the different ranges of the IFP. (b) Half-logarithmic plot of the IFP data to the left of the first peak (squares). The best linear fit to the data is also shown (line). (c) The same as in (b) but for the IFP data to the right of the second peak (triangles). On this side, the decay of the IFP saturates due to the background fluorescence. The data after the saturation are not included (see (a)). (d) Half-logarithmic plot of the computed IFP, $I(u)$, for a cell model with a Z-ring that is $0.3 \mu\text{m}$ wide (squares, see the text). Here, the IFP was normalized such that $I(0) = 1$. Since the best fitting line to $I(u)$ in the range $2.5 \times 10^{-2} < I < 0.85$ cannot be distinguished from $I(u)$ itself, it was shifted upward (line).

length scale, respectively, for the contribution of each of these formations to the IFP.

Since in the focal plane the PSF is well approximated by a Gaussian, the exponential decay of the Z-ring IFPs was surprising. However, a significant fraction of the Z-ring lies far from the focal plane where the Gaussian approximation to the PSF is no longer valid. As we move away from the focal plane, the secondary lobes of the PSF grow relative to the central peak and their average amplitude decays at a gradually slower rate (supplementary figure 1 available at stacks.iop.org/PhysBio/8/066003/mmedia). For our optical system, starting at about $0.3 \mu\text{m}$ from the focal plane, the PSF(r) oscillates around a decaying average that is approximately exponential (see the supplementary material available at stacks.iop.org/PhysBio/8/066003/mmedia). Therefore, the off-focus contributions to the Z-ring image are those that dominate the behavior in the tails and determine their exponential decay. To verify this scenario, we simulated the behavior of the IFP for a

cell model. In our model, the cell was shaped as a cylinder with hemispherical caps (cell length, L , was $3 \mu\text{m}$ and cell radius, R , was $0.5 \mu\text{m}$). The Z-ring of the model cell consisted of an open-ended cylindrical surface of radius $0.49 \mu\text{m}$ and length Δ . This cylindrical surface was centered at midcell such that its axis coincided with the long cell axis. We used a theoretical 3D PSF model appropriately adjusted for our large NA objective [45]. To obtain the model IFP, we convoluted the 3D PSF with the Z-ring of the model and integrated the focal plane section of the resulting 3D image across the cell width. Here, we assumed that the focal plane coincided with the cell midplane. The outcome of this procedure for $\Delta = 0.3 \mu\text{m}$ is shown in figure 3(d). The value of Δ used in figure 3(d) is consistent with a recent estimation of the Z-ring width obtained by using high-resolution imaging [46]. Note that in the experimentally relevant range, i.e. $I > 2 \times 10^{-2} I(u = 0)$, as a good approximation, $I(u)$ decays exponentially, with the exception of a small range around $u = 0$. Although for smaller ring widths, Δ , the decay of

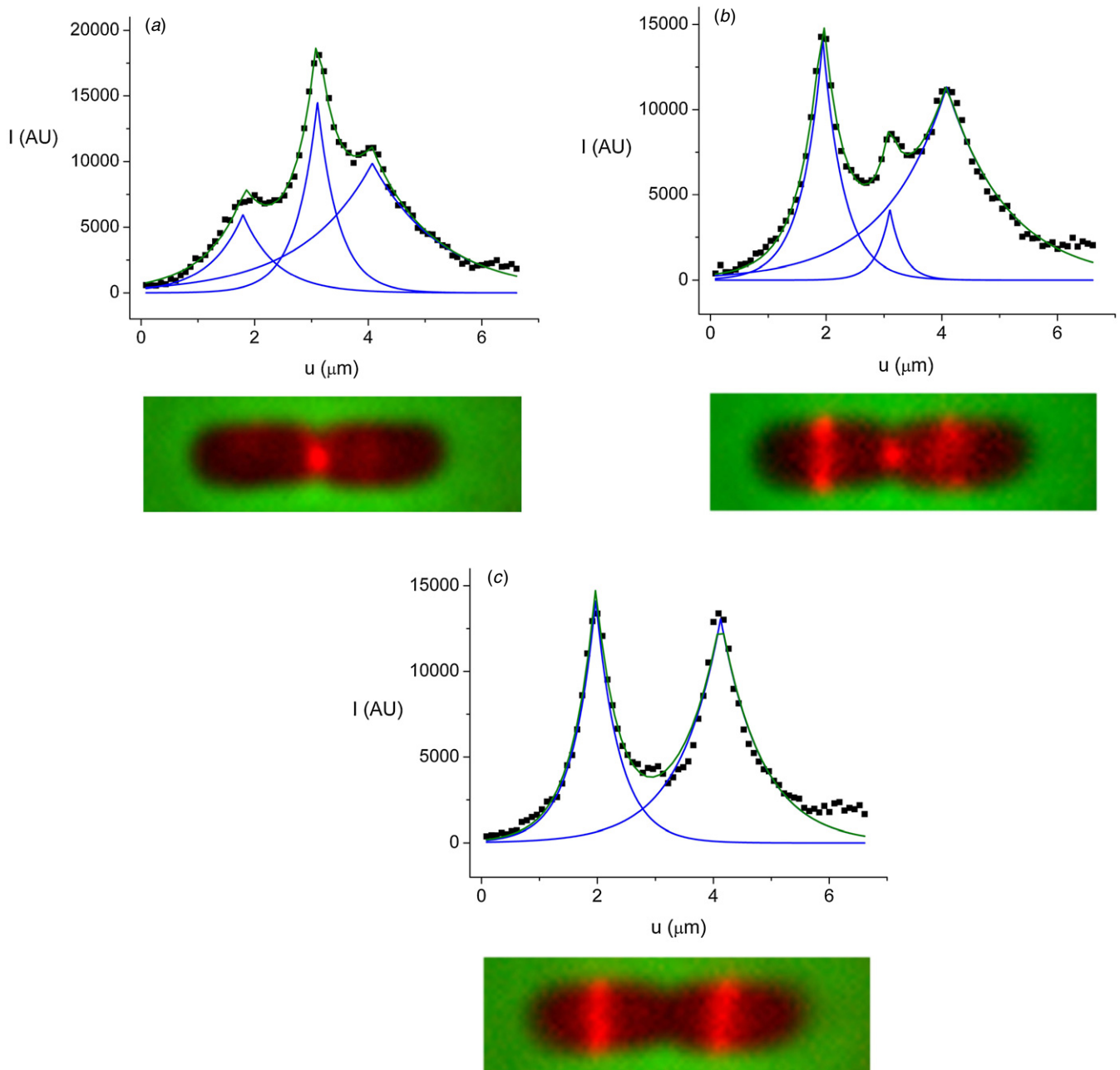


Figure 4. FtsZ-GFP dynamics from a zoom experiment and the corresponding IFPs (squares) for the same cell as in figure 3; the IFP of figure 3(a) is the same as that of figure 4(c). The images are overlays of a fluorescence frame (red) with the previous phase-contrast frame (green). The IFPs are shown together with the best fits of equation (1) (green) and the corresponding decomposition into exponential peaks (blue). (a) $t = 1.33$ min, (b) $t = 2.00$ min and (c) $t = 2.87$ min, where time was measured from the start of the time-lapse experiment. All three images and their corresponding IFPs have the same length scale. Moreover, the three images show the same region in the sample. The IFPs were computed starting from the left edge of the image and ending at the right edge. The fluorescence beyond the cell caps is due to either background fluorescence or the diffractive tails of the FtsZ-GFP distribution.

$I(u)$ was somewhat oscillatory (see supplementary material available at stacks.iop.org/PhysBio/8/066003/mmedia), its average remained exponential.

To show that equation (1) provides an accurate description of the FtsZ-GFP distribution, we used it to analyze the IFP dynamics in a zoom experiment. In figure 4, we show images of an *E. coli* cell at different stages of Z-ring formation. Each image is the result of the overlay of a fluorescence frame with the previous phase-contrast frame. The corresponding

IFPs together with the best fitting $f(u)$ of equation (1) are also shown. Note the good agreement between $f(u)$ and the data. In figure 4(a), the mother cell was approaching the end of its division and its Z-ring was already much smaller than the full cell width. The IFP revealed that there were already FtsZ formations in the central sections of the daughter cells. As little as 40 s later (figure 4(b)), the Z-rings of the daughter cells had already attained a higher IFP weight than that of the mother. Note that the rightmost ring was still relatively diffuse.

Finally, 52 s later (figure 4(c)), the Z-ring of the mother cell had disappeared, and only the Z-rings of the daughter cells could be detected. Overlapping dynamics of Z-rings in mother and daughter cells, showing in figure 4 as three coexisting Z-rings, were also noted by Sun and Margolin [47]. Such behavior appears to be typical for cells with short division cycles.

3.2. Establishing τ_z , the Z-ring localization time

The analysis of the timing in the low-induction experiments was slightly different from that of figure 4. Here, we followed the morphogenesis and FtsZ-GFP dynamics throughout the life cycle of a particular cell. Since we analyzed each of the daughter cells separately, we assumed a single FtsZ-GFP structure and thus used equation (1) with $N = 1$. To avoid the interference from the remains of the old Z-ring, we used only the middle half of the cell for the fit. The background due to the cytoplasmic FtsZ-GFP was approximated by the average fluorescence intensity in the old cell cap and subtracted throughout the cell.

To determine the time at which a particular Z-ring had stabilized, we monitored the position of its IFP peak, $u_1(t)$ (figure 5(a), and supplementary figures 3(a) and 4(a) available at stacks.iop.org/PhysBio/8/066003/mmedia). As discussed in the introduction, the Z-ring is expected to assemble around midcell (where the concentration of MinC is sufficiently reduced) at a time at which the new nucleoids have moved toward the centers of the future daughter cells. Indeed, we found that $u_1(t)$ typically displayed large oscillations at the beginning of the cell cycle and that soon these oscillations decayed to an almost fixed value. Computer simulations of cellular FtsZ dynamics ([48] and supplementary material available at stacks.iop.org/PhysBio/8/066003/mmedia) suggested that these oscillations were due to FtsZ arcs or rings that formed outside the cellular midplane and were periodically dissolved by membrane-associated MinC prior to Z-ring formation (see figure 5(b)). These arcs represent clusters of membrane-bound FtsZ polymers. The model assumes that the membrane-bound FtsZ polymers are exclusively aligned in circumferential orientation⁷ and all polymers are taken to be of the same length, which is 125 nm (~ 30 subunits). This is the average polymer length observed in *in vitro* experiments at physiological concentration [50]. Cluster formation is mediated by lateral and end-to-end contacts between the FtsZ polymers. When FtsZ arcs hit the cell middle, a complete Z-ring forms and is stable in this position. We therefore defined τ_z as the time of the transition between the oscillatory and the stable regime of $u_1(t)$. Specifically, to define τ_z , we used the standard deviation (Sd) of the measured $u_1(t)$ values. $Sd_t(u_1(t))$ represents the average variation of $u_1(t)$ between consecutive frames as a function of the time along the cell cycle. Then, τ_z corresponds to the time at which $Sd_t(u_1(t))$ decreases to a relatively small value. The details of this analysis are described in the supplementary material available at stacks.iop.org/PhysBio/8/066003/mmedia.

⁷ The choice of circumferential orientation is supported by cryo-EM observations of FtsZ in *Caulobacter crescentus* [49]. It is possible that this orientation is enforced by the spontaneous curvature of FtsZ polymers.

In addition to the dynamics of the center of the FtsZ-GFP distribution, in figure 5(a) we also show the FtsZ-GFP image and the corresponding IFP at two times, $t_1 < \tau_z$ and $t_2 = \tau_z$. Since both t_1 and t_2 belong to a transitional regime, the FtsZ-GFP distribution was relatively disperse at these times. As suggested by the simulations, at t_1 , with the exception of the FtsZ-GFP that belonged to the old ring, the rest of the FtsZ-GFP was located in a band around $u/L \approx 0.3$. Excluding the contribution from the old ring, the exponential fit to the IFP measured the center of this band. In contrast, at $t_2 = \tau_z$ most of the FtsZ-GFP was already located at midcell, although the Z-ring still appeared to be incomplete.

Another parameter that may indicate whether the Z-ring has already formed is the width of the corresponding IFP peak. As a measure of this width, we used the standard deviation of the best fitting exponential peak, $Sd_{IFP} = \sqrt{2}k_1$. Note that Sd_{IFP} and $Sd_t(u_1(t))$ correspond to manifestly different properties of the IFP: While Sd_{IFP} measures the spread of the IFP along the cell at a particular time, $Sd_t(u_1(t))$ monitors the temporal fluctuations of the center of the IFP, $u_1(t)$. In figure 6(a), and supplementary figures 3(b) and 4(b) available at stacks.iop.org/PhysBio/8/066003/mmedia, we show the width dynamics, $Sd_{IFP}(t)$, for the same cells as in figure 5(a), and supplementary figures 3(a) and 4(a) available at stacks.iop.org/PhysBio/8/066003/mmedia, respectively. The behavior of $Sd_{IFP}(t)$ appeared to be similar to that of $u_1(t)$, namely, after a few wide oscillations, it settled down to an almost constant value. This finding is consistent with the Z-ring maturing via the condensation of a relatively diffuse FtsZ membrane-anchored structure. However, unlike the positioning dynamics, we found that for several cells, $Sd_{IFP}(t)$ displayed oscillations of about the same size throughout the cell cycle. This finding suggests that we may not rely on $Sd_{IFP}(t)$ to determine τ_z . A possible explanation for the above behavior lies in the predictions of computer simulations of FtsZ dynamics (see figure 6(b)) [48]. The computer simulations showed that small polar FtsZ arcs continue to form outside the cellular midplane after τ_z . These arcs, which are dissolved quickly by Min proteins, add little to the center of mass of the FtsZ distribution, but make a significant contribution to the standard deviation due to their potentially large distance from the cell middle. Therefore, the standard deviation of the FtsZ distribution can fluctuate and take large values after Z-ring formation. This scenario was supported by our low-induction experiments. For example, in figure 6(a), we show that such an off-center arc was present, albeit weakly, at $t = 8.15$ min, leading to an increased value of Sd_{IFP} , while u_1/L was almost unaffected (figure 5(a)).

3.3. Correlations between τ_z and the septation parameters, τ_c , τ_g and L_0

Using our IFP peak dynamics approach, we determined τ_z for all the cells of the low-induction experiments (figure 1 and table 1). In addition, τ_c , τ_g and L_0 were measured for these cells from the phase-contrast part of the time-lapse recording (figure 1 and table 1). This information enabled us to test for correlations between the time of Z-ring positioning and time and length scales related to septation.

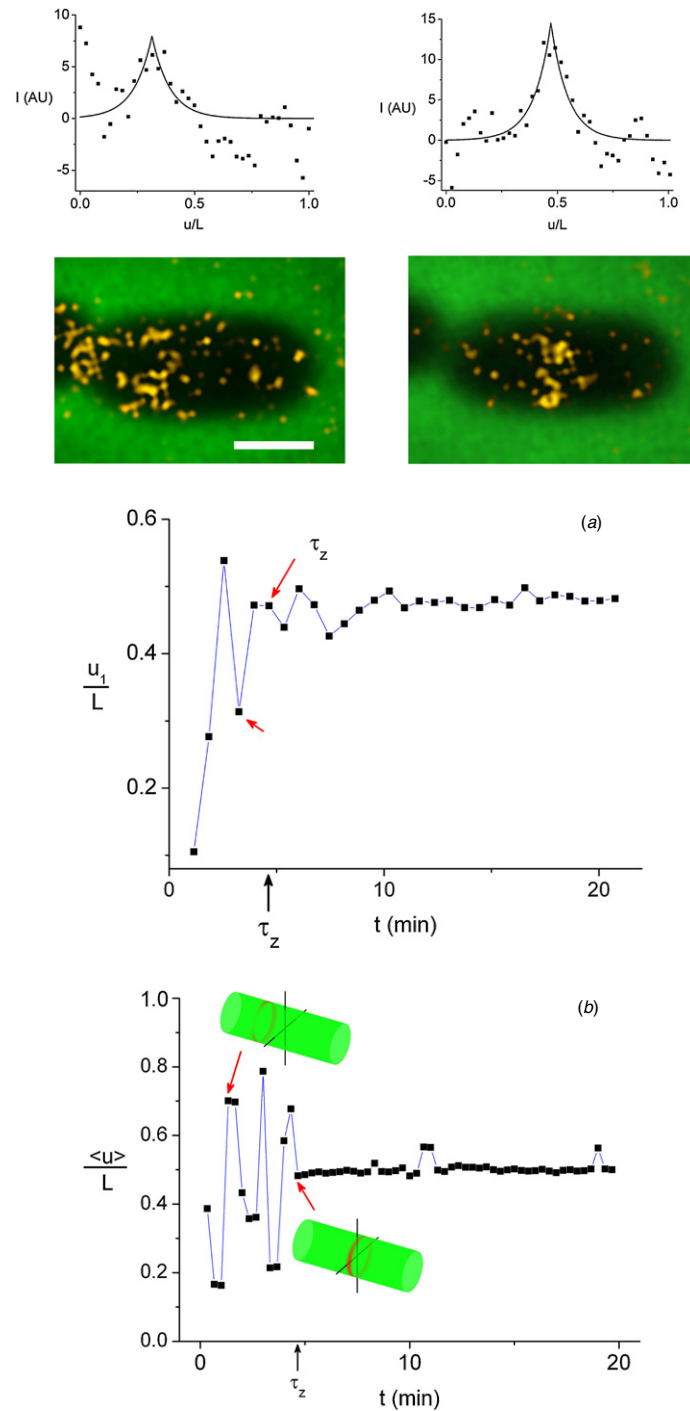


Figure 5. Position dynamics of the FtsZ-GFP distribution. (a) For a cell from a low-induction experiment (line with squares). The position of the FtsZ-GFP distribution corresponds to the peak of the best fitting exponential to the IFP, u_1 , and is normalized to the cell length, L . Time is measured from cell birth to the end of division. The imaged FtsZ-GFP distribution and the corresponding IFP, $I(u/L)$, are shown at two times, $t = 3.25$ min (short arrow) and $t = \tau_z = 4.65$ min (long arrow). For $t < \tau_z$ (left), most of the FtsZ-GFP was localized either in an off-center band or at the position of the old ring. At $t = \tau_z$ (right), most of the FtsZ-GFP was localized around midcell. The 2D FtsZ-GFP distributions were obtained from the overlay of a fluorescence cell image (yellow) with the preceding phase-contrast image (green). To emphasize the localization pattern of the FtsZ-GFP, we applied a high threshold on the fluorescence part of the image, which leads to a fragmented appearance of the 2D FtsZ-GFP distribution. We stress that the IFPs were obtained directly from the unprocessed fluorescence image. Bar = $1 \mu\text{m}$. To exclude the effect of the old ring, the IFP data (squares) were fitted with a single exponential only in the $0.25 < u/L < 0.75$ range (line). (b) Results of a computer simulation of FtsZ dynamics in a cylindrical *in silico* bacterium [48], including Min oscillations (period 80 s). FtsZ concentrations were projected on the long axis of the bacterium. Shown is the position of the center of mass (normalized to cell length, L) of membrane-bound FtsZ as a function of time, $\langle u \rangle / L$. The small cylinder images show a snapshot of the FtsZ distributions at the times indicated by the red arrows, illustrating that the oscillations arise due to transient arcs/rings forming off the cellular midplane. Regions of high FtsZ concentrations are depicted in red, and regions void of FtsZ are depicted in green. The cylinder midplane is indicated by a black axis cross.

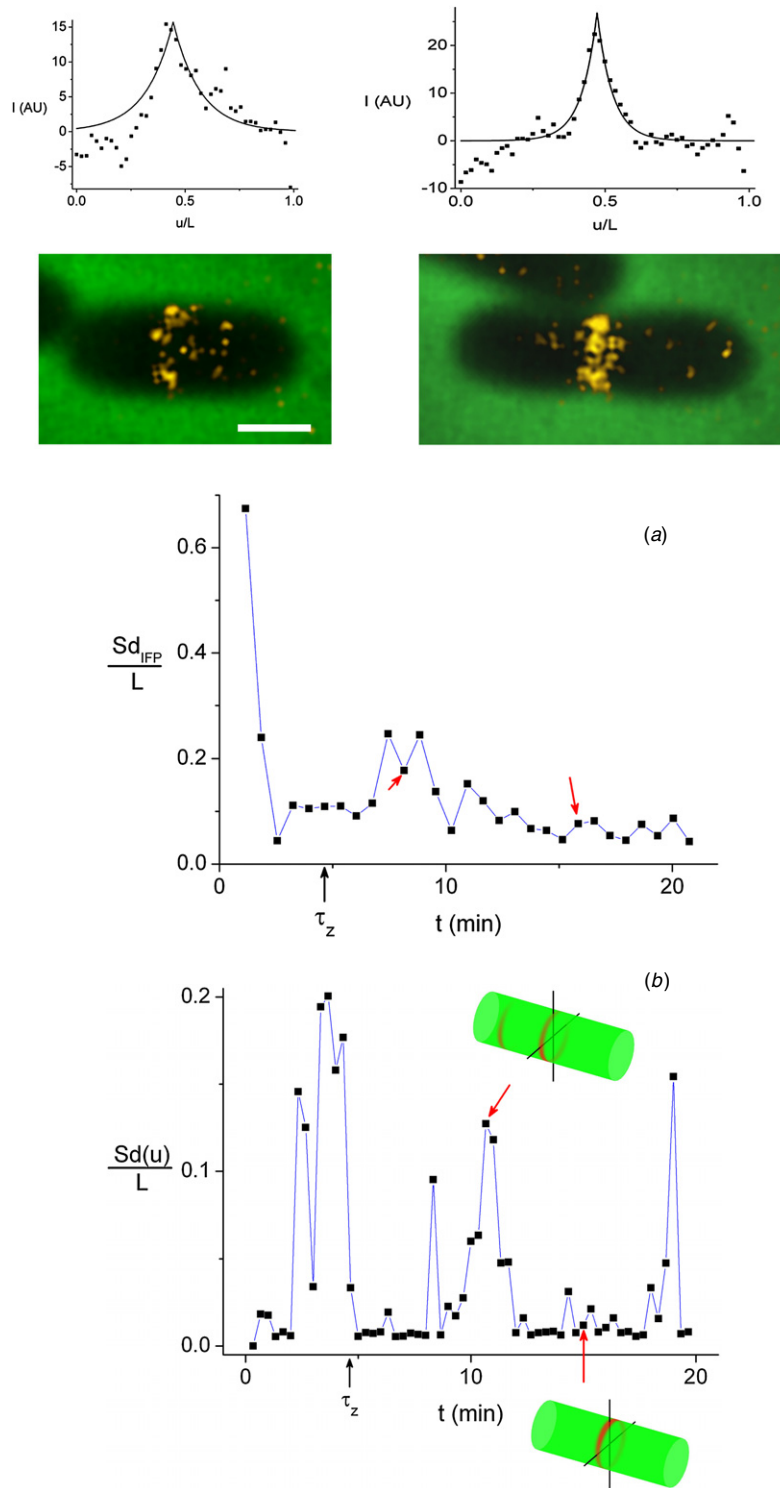


Figure 6. Width dynamics of the FtsZ-GFP distribution. (a) For the same cell as in figure 5(a) (line with squares). The width, Sd_{IFP} , corresponds to the standard deviation of the best fitting exponential to the IFP. As in figure 5(a), the imaged FtsZ-GFP distribution and the corresponding IFP, $I(u/L)$, are shown at two times, $t = 8.15$ min (short arrow) and $t = 15.85$ min (long arrow). For the former (left), although most of the FtsZ-GFP is localized around midcell, there is a weak additional band at $u/L \approx 0.7$. This additional band can be seen in both the FtsZ-GFP image and in its IFP. While this band has little effect on the center of mass of the IFP, u_1/L , it leads to an increased value of its normalized width, Sd_{IFP}/L . At the later time, $t = 15.85$ min (right), the FtsZ-GFP distribution represents an established single Z-ring. Note the good agreement between the IFP data and the corresponding exponential best fit. Bar = $1 \mu\text{m}$. (b) Results of the same computer simulation of FtsZ dynamics as in figure 5(b). Shown is the standard deviation of membrane-bound FtsZ along the cell axis normalized to cell length, Sd/L , as a function of time. The small cylinder images show a snapshot of the FtsZ distributions at the times indicated by the red arrows, illustrating that the fluctuations arise due to transient arcs forming off the cellular midplane, even after the stable Z-ring has formed at the cell center. Regions of high FtsZ concentrations are depicted in red, and regions void of FtsZ are depicted in green. The cylinder midplane is indicated by a black axis cross.

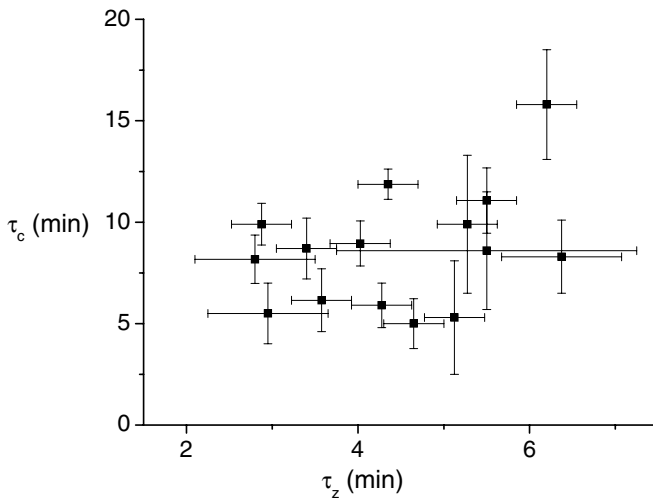


Figure 7. Lack of correlation between the Z-ring localization time, τ_z , and that for the onset of septation, τ_c . The data of the $\tau_z(\tau_c)$ plot (squares) are for the 15 cells from the low-induction experiments.

Table 1. Average timescales and their variabilities for the population of 15 cells analyzed in the low-induction experiments.

Parameter	Mean (min)	Sd (min)	CV ^a (%)
τ_g	22.16	2.97	13.4
τ_c	8.61	2.92	34
τ_z	4.46	1.19	26
$\tau_g - \tau_z$	17.70	2.67	15
$\tau_c - \tau_z$	4.15	2.71	65
$\tau_g - \tau_c$	13.55	2.67	20

^a CV = coefficient of variation.

As discussed in the introduction, using the image analysis methods developed in [39], we found that the onset of division occurs much earlier than the time at which the beginning of the constriction can be established visually, τ_{cv} . On average, for cells with $\langle \tau_g \rangle \cong 24$ min, τ_c was about 5 min smaller than τ_{cv} . Moreover, both τ_z and τ_c displayed significant variability ($CV(\tau_z) = 26\%$ and $CV(\tau_c) = 34\%$). Nevertheless, for each of the cells of the low-induction experiments, Z-ring positioning took place before the onset of septation, $\tau_z < \tau_c$. This result provides further support for the validity of our single-cell approach for establishing the time of Z-ring positioning, τ_z .

The time of Z-ring localization divides the interval from cell birth to the onset of septation, τ_c , into two different periods. While the first period, $(0, \tau_z)$, is associated with the positioning of the Z-ring, the second period, (τ_z, τ_c) , stretches from Z-ring localization to the onset of septation. We found that there was apparently no correlation between the extent of the first period, τ_z , and either τ_c (see figure 7) or τ_g (not shown); this finding indicates that Z-ring positioning has no direct influence on the onset of septation.

To probe the nature of the (τ_z, τ_c) period, we tested the Z-ring position stability in the different time regimes. We found that the fluctuations of $u_1(t)$ were significantly larger for $\tau_z < t < \tau_c$ than for $\tau_c < t < \tau_g$. Specifically, while the average standard deviation of $u_1(t)/L$ was 0.033 for the former time interval, it was as little as 0.014 for the latter. In

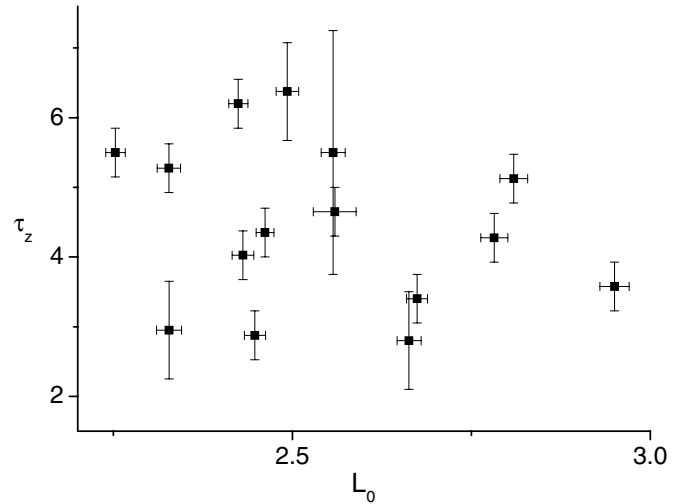


Figure 8. Lack of correlation between the Z-ring localization time, τ_z , and the cell length at birth, L_0 . The data of the $L_0(\tau_z)$ plot (squares) are for the 15 cells of the low-induction experiments.

fact, $Sd(u_1(t)/L)$ was smaller during the T-period than in the $\tau_z < t < \tau_c$ interval for each individual cell. The increase in Z-ring stability following the onset of septation may be attributed to its association with the growing constriction of the peptidoglycan layer.

In previous work, we have shown that a compensation mechanism controls the cell length variability [40]. Specifically, we found that the time for the onset of septation, τ_c , was larger for cells that were shorter at birth. In contrast, here we found that there is apparently no correlation between the Z-ring positioning time, τ_z , and the cell length at birth, L_0 (see figure 8). This finding suggests that the timescale of the Z-ring positioning mechanism is not affected by the cell length.

4. Discussion

We used time-lapse microscopy to monitor individual *E. coli* cells over their entire life cycle. The imaging mode was automatically switched between phase-contrast and fluorescence. While the phase-contrast mode was used to examine cell cytokinesis, the fluorescence mode enabled us to follow FtsZ-GFP dynamics and the localization of the Z-ring at midcell. For the analysis of the fluorescence images, we employed the IFP, which integrates the fluorescence intensity across the width of the cell. We found that the IFP of a Z-ring is well approximated by an exponentially decaying distribution. It was shown that this behavior of the IFP may be attributed to an exponential range of the PSF far enough from the focal plane.

Using the IFP, we identified the moment of significant change in the positional stability of the Z-ring and defined it as the Z-ring positioning time, τ_z . The pattern of Z-ring positional dynamics, i.e. oscillations before τ_z and sharp stabilization thereafter, was observed for all analyzed cells and is best illustrated in a rescaled representation (supplementary figure 6 available at stacks.iop.org/PhysBio/8/066003/mmedia).

The identification of the Z-ring positioning event was corroborated also by comparison with simulations of a computational model for FtsZ dynamics [48]. The Z-ring positioning, together with the onset of septation and the end of division, form three of the main events of bacterial cell division (figure 1). We found that for all the cells of the low-induction experiments, Z-ring positioning occurred before the beginning of constriction, $\tau_z < \tau_c$. Moreover, the time of Z-ring positioning, τ_z , was apparently independent of the septation timescales, τ_c and τ_g , and of the cell length at birth, L_0 . We also showed that the position of the Z-ring was more stable during the T-period, $\tau_c < t < \tau_g$, than during the (τ_z, τ_c) period.

Two alternative methods to establish the time of Z-ring formation were tested. In the first approach, we used the dynamics of the standard deviation of the IFP, $Sd_{IFP}(t)$, to find the time when the FtsZ-GFP cloud condenses into a relatively thin Z-ring (see figure 6(a), and supplementary figures 3(b), 4(b) and 7(b) available at stacks.iop.org/PhysBio/8/066003/mmedia). While for most of the cells we find that $Sd_{IFP}(t)$ exhibits a transition between a regime of wide oscillations to one of relatively low values that occurs at times close to τ_z (figure 6(a), and supplementary figures 3(b) and 4(b) available at stacks.iop.org/PhysBio/8/066003/mmedia), in others such a transition is not apparent (supplementary figure 7(b) available at stacks.iop.org/PhysBio/8/066003/mmedia). Both experiment (figure 6(a)) and computer simulations (figure 6(b)) suggest that the large values of $Sd_{IFP}(t)$ at times beyond τ_z may be due to the formation of transient off-center FtsZ-GFP structures on the cytoplasmic membrane. Since such structures have a significantly larger effect on the values of $Sd_{IFP}(t)$ than on those of $u_1(t)$, the former is not useful for timing Z-ring formation. A second approach consisted of monitoring the fluorescence intensity at midcell throughout the cell cycle (supplementary figure 7(c) available at stacks.iop.org/PhysBio/8/066003/mmedia). We defined the intensity at midcell, I_{mid} , as the average of the IFP values in the 3 pixels around the center of the cell and plotted I_{mid} as a function time for each of the low-induction cells. It was expected that before Z-ring positioning, I_{mid} would grow reaching a certain saturation level at τ_z . As for the case of $Sd_{IFP}(t)$, we found that while for some cells this is indeed the observed behavior of $I_{mid}(t)$, for others the dynamics is much more complex (see e.g. supplementary figure 7(c) available at stacks.iop.org/PhysBio/8/066003/mmedia). The fact that the fluorescence intensity at midcell is less robust than the IFP positional dynamics could be due to either variations in the expression level of the FtsZ-GFP throughout the cell cycle or GFP bleaching.

The apparent lack of correlation between τ_z and either τ_c or τ_g indicates that the mechanism of Z-ring assembly and localization and that of septation are not directly dependent on one another. While the former consists of an assembly mechanism for FtsZ filaments into the Z-ring controlled by the MinCDE and nucleoid occlusion systems, the latter involves the recruitment of the septal peptidoglycan building machinery to commence envelope constriction. The dynamic

independence of these two mechanisms is consistent with the two-step divisome maturation concept [37].

Additional evidence that septation and Z-ring positioning are two distinct mechanisms may be drawn from the fact that τ_z appears to be uncorrelated with the cell length at birth, L_0 (figure 8). In this respect, τ_z differs from τ_c in that the latter was shown to be negatively correlated with L_0 , leading to a compensation mechanism that controls the population variability of cell lengths [40]. Specifically, in cells that are shorter at birth, the onset of septation is postponed, allowing these cells to reach a certain range of cell lengths before they start to divide.

It is worthwhile to compare the time interval between Z-ring positioning and the onset of septation, $\tau_c - \tau_z$, and that of the divisome assembly. We define the latter as the time between the following two events: (1) binding of the first non-FtsZ proteins to the Z-ring, τ_A , and (2) the addition of FtsN to the Z-ring, τ_N . The average values of τ_N and the visible onset of septation, τ_{cv} , were measured in [37] for cell populations with different growth rates. Using the appropriate correction to obtain the corresponding value of τ_c [39], we found that τ_N and τ_c were practically identical within experimental error. Moreover, since it has been shown that FtsZ, FtsA, ZipA [51, 38, 52] and ZapA [53] localize at midcell at approximately the same time, it is reasonable to assume that the $\tau_c - \tau_z$ interval that we measured overlaps considerably with divisome assembly. Although our results do not provide new evidence to support this assumption, it is useful to discuss its implications.

As discussed in the introduction, divisome assembly is a sequential process whereby a large number of proteins join the Z-ring in a particular order, with each step in this process depending on the completion of the previous step. Moreover, most of the divisome proteins are present in a small number of copies per cell and to adhere to the Z-ring, the proteins may have to diffuse over significant fractions of the cell volume. The cumulative time variability of the assembly together with the large variability of the individual steps leads to the large CV of the divisome assembly time and correspondingly of $\tau_c - \tau_z$ (table 1).

Cells with longer divisome assembly periods will accumulate more copies of FtsW and FtsI (PBP3) in the divisome and are likely to septate faster. We have previously shown that the rate of septal growth, $2a_h$, can be obtained from the cell radius, R , and the radius of the constriction, $r(t)$, by using a simple geometrical model [39]. Due to the small variation range of a_h , the correlation found between a_h and $\tau_c - \tau_z$ was rather noisy. Nevertheless, we suggest that the increase of a_h with $\tau_c - \tau_z$ represents a true trend, which is more pronounced for cells with comparable generation times, τ_g (see supplementary figure 8 available at stacks.iop.org/PhysBio/8/066003/mmedia). Therefore, a shorter T-period, $\tau_g - \tau_c$, compensates for slower divisome formation, $\tau_N - \tau_A$, and the resulting delay in the onset of septation.

The average $\tau_c - \tau_z$ of 4.15 min in our measurements differed from the value for the divisome assembly period $\tau_N - \tau_A$ obtained by Aarsman *et al* [37]. They found a clear linear relation between the divisome assembly time and the

growth rate. Extrapolating this dependence to the growth rate of our cells (22.16 min) gives a value of 12.7 min, i.e. about three times longer than our average $\tau_c - \tau_z$. This apparent discrepancy could be due to a number of factors. First, it may stem from the different ways in which the times were measured, namely, Aarsman *et al* [37] used population statistics methods, whereas we used a dynamic single-cell approach. Second, the discrepancy may be due to higher concentrations of the divisome components at faster growth due to the multiple chromosome equivalents per cell. On one hand, Aarsman *et al* [37] showed that overproduction of at least one protein, FtsN, did not influence the length of the $\tau_N - \tau_A$ period. On the other hand, there is some evidence for non-sequential assembly of divisome components [35, 36], which may accelerate the overall process by assembling sub-complexes. Third, our bacterial strain and growth temperature are different from those of Aarsman *et al* [37].

Finally, using the IFP to study the FtsZ-GFP dynamics, we reduced the 2D fluorescence intensity distribution of FtsZ-GFP in the cell to a 1D function that can be more readily analyzed. We should, however, remember that this approach conceals most of the fine structure of the FtsZ-GFP distribution, e.g., helical formations. We expect that a quantitative analysis of the full 2D FtsZ-GFP distribution will reveal additional features of the Z-ring formation process.

Acknowledgments

We thank Y Garini, Y Meir and O Piro for useful discussions and D S Weiss for the bacterial strain. This research was supported in part by the Israel Academy of Science and Humanities (grant nos 820/05 and 1544/08), the BSF (grant no 2006285 to NSG) and the Minerva Foundation (grant no 710589 to NSG and a postdoc scholarship to EFF).

References

- [1] Errington J, Daniel R A and Dirk-Jan S 2003 Cytokinesis in bacteria *Microbiol. Mol. Biol. Rev.* **67** 52–65
- [2] Margolin W 2000 Themes and variations in prokaryotic cell division *FEMS Microbiol. Rev.* **24** 531–48
- [3] Nanninga N 2001 Cytokinesis in prokaryotes and eukaryotes: common principles and different solutions *Microbiol. Mol. Biol. Rev.* **65** 319–33
- [4] Rothfield L, Justice S and Garcia-Lara J 1999 Bacterial cell division *Annu. Rev. Genet.* **33** 423–48
- [5] Nanninga N 1998 Morphogenesis of *Escherichia coli* *Microbiol. Mol. Biol. Rev.* **62** 110–29
- [6] Dajkovic A and Lutkenhaus J 2006 Z-ring as executor of bacterial cell division *J. Mol. Microbiol. Biotechnol.* **11** 140–51
- [7] den Blaauwen T, de Pedro M A, Nguyen-Distèche M and Ayala J A 2008 Morphogenesis of rod-shaped sacculi *FEMS Microbiol. Rev.* **32** 321–44
- [8] Adams D W and Errington J 2009 Bacterial cell division: assembly, maintenance and disassembly of the Z-ring *Nat. Rev. Microbiol.* **7** 642–53
- [9] Bi E and Lutkenhaus J 1991 FtsZ ring structure associated with division in *Escherichia coli* *Nature* **354** 161–4
- [10] Addinall S and Lutkenhaus J 1996 FtsZ-spirals and -arcs determine the shape of the invaginating septa in some mutants of *Escherichia coli* *Mol. Microbiol.* **22** 231–7
- [11] Levin P and Losick R 1996 Transcription factor Spo0A switches the localization of the cell division protein FtsZ from a medial to a bipolar pattern in *Bacillus subtilis* *Genes Dev.* **10** 478–8
- [12] Trueba F J and Woldringh C L 1980 Changes in cell diameter during the division cycle of *Escherichia coli* *J. Bacteriol.* **142** 869–78
- [13] de Boer P A J, Crossley R E and Rothfield L I 1989 A division inhibitor and a topological specificity factor coded for by the minicell locus determine the proper placement of the division site in *Escherichia coli* *Cell* **56** 641–9
- [14] Lutkenhaus J and Sundaramoorthy M 2003 MinD and role of the deviant Walker A motif, dimerization and membrane binding in oscillation *Mol. Microbiol.* **48** 295–303
- [15] Mulder E and Woldringh C L 1989 Actively replicating nucleoids influence positioning of division sites in *Escherichia coli* filaments forming cells lacking DNA *J. Bacteriol.* **171** 4303–14
- [16] Woldringh C L, Mulder E, Huls P G and Vischer N 1991 Toporegulation of bacterial division according to the nucleoid occlusion model *Res. Microbiol.* **142** 309–20
- [17] Fu X, Shih Y L, Zhang Y and Rothfield L I 2001 The MinE ring required for proper placement of the division site is a mobile structure that changes its cellular location during the *Escherichia coli* division cycle *Proc. Natl Acad. Sci. USA* **98** 980–5
- [18] Hu Z and Lutkenhaus J 1999 Topological regulation of cell division in *Escherichia coli* involves rapid pole to pole oscillation of the division inhibitor MinC under the control of MinD and MinE *Mol. Microbiol.* **34** 82–90
- [19] Raskin D M and de Boer P A J 1999 MinDE-dependent pole-to-pole oscillation of division inhibitor MinC in *Escherichia coli* *J. Bacteriol.* **181** 6419–24
- [20] Raskin D M and de Boer P A J 1999 Rapid pole-to-pole oscillation of a protein required for directing division to the middle of *Escherichia coli* *Proc. Natl Acad. Sci. USA* **96** 4971–6
- [21] Meinhardt H and de Boer P A J 2001 Pattern formation in *Escherichia coli*: a model for the pole to-pole oscillations in min proteins and the localization of the division site *Proc. Natl Acad. Sci. USA* **98** 14202–7
- [22] Kruse K 2002 A dynamic model for determining the middle of *Escherichia coli* *Biophys. J.* **82** 618–27
- [23] Huang K C, Meir Y and Wingreen N S 2003 Dynamic structures in *Escherichia coli*: spontaneous formation of MinE rings and MinD polar zones *Proc. Natl Acad. Sci. USA* **100** 12724–8
- [24] Howard M and Rutenberg A D 2003 Pattern formation inside bacteria: fluctuations due to the low copy number of proteins *Phys. Rev. Lett.* **90** 128102
- [25] Kerr R A, Levine H, Sejnowski T J and Rappel W-J 2006 Division accuracy in stochastic model of Min oscillations in *Escherichia coli* *Proc. Natl Acad. Sci. USA* **103** 347–52
- [26] Wu L J and Errington J 2004 Coordination of cell division and chromosome segregation by a nucleoid occlusion protein in *Bacillus subtilis* *Cell* **117** 915–25
- [27] Bernhardt T G and de Boer P A J 2005 SlmA, a nucleoid-associated, FtsZ binding protein required for blocking septal ring assembly over chromosomes in *E. coli* *Mol. Cell.* **27** 555–64
- [28] Lan G, Wolgemuth C W and Sun S X 2007 Z-ring force and cell shape during division in rod-like bacteria *Proc. Natl Acad. Sci. USA* **104** 16110–5
- [29] Ghosh B and Sain A 2008 Origin of contractile force during cell division of bacteria *Phys. Rev. Lett.* **101** 178101

- [30] Shlomovitz R and Gov N S 2009 Membrane mediated interactions drive the condensation and coalescence of FtsZ rings *Phys. Biol.* **6** 046017
- [31] Lan G, Daniels B R, Dobrowsky T M, Wirtz D and Sun S X 2009 Condensation of FtsZ filaments can drive bacterial cell division *Proc. Natl Acad. Sci. USA* **106** 121–6
- [32] Allard J F and Cytrynbaum E N 2009 Force generation by a dynamic Z-ring in *Escherichia coli* cell division *Proc. Natl Acad. Sci. USA* **106** 145–50
- [33] Thanedar S and Margolin W 2004 FtsZ exhibits rapid movement and oscillation waves in helix-like patterns in *Escherichia coli* *Curr. Biol.* **14** 1167–73
- [34] Peters P C, Migocki M D, Thoni C and Harry E J 2007 A new assembly pathway for the cytotkinetic Z-ring from a dynamic helical structure in vegetatively growing cells of *Bacillus subtilis* *Mol. Microbiol.* **64** 487–99
- [35] Goehring N W, Gueiros-Filho F and Beckwith J 2005 Premature targeting of a cell division protein to midcell allows dissection of divisome assembly in *Escherichia coli* *Genes Dev.* **19** 127–37
- [36] Goehring N W, Gonzalez M D and Beckwith J 2006 Premature targeting of cell division proteins to midcell reveals hierarchies of protein interactions involved in divisome assembly *Mol. Microbiol.* **61** 33–45
- [37] Aarsman M E G, Piette A, Fraipont C, Vinkenvleugel T M F, Nguyen-Distèche M and den Blaauwen T 2005 Maturation of the *Escherichia coli* divisome occurs in two steps *Mol. Microbiol.* **55** 1631–45
- [38] den Blaauwen T, Buddelmeijer N, Aarsman M E G, Hameete C M and Nanninga N 1999 Timing of FtsZ assembly in *Escherichia coli* *J. Bacteriol.* **181** 5167–75
- [39] Reshes G, Vanounou S, Fishov I and Feingold M 2008 Cell shape dynamics in *E. coli* *Biophys. J.* **94** 251–64
- [40] Reshes G, Vanounou S, Fishov I and Feingold M 2008 Timing the start of division in *E. coli*: single cell study *Phys. Biol.* **5** 046001
- [41] Guberman J M, Fay A, Dworkin J, Wingreen N S and Gitai Z 2008 PSICIC: noise and asymmetry in bacterial division revealed by computational image analysis at sub-pixel resolution *PLoS Comput. Biol.* **4** e1000233
- [42] Weiss D S, Chen J C, Ghigo J-M, Boyd D and Beckwith J 1999 Localization of FtsI (PBP3) to the septal ring requires its membrane anchor, the Z-ring, FtsA, FtsQ and FtsI *J. Bacteriol.* **181** 508–20
- [43] Young I T, Zagers R, van Vliet L J, Mullikin J, Boddeke F and Netten H 1993 Depth-of-focus in microscopy *SCIA'93: Proc. 8th Scandinavian Conf. on Image Analysis (Tromso, Norway, 1993)* pp 493–8
- [44] Itan E, Carmon G, Rabinovitch A, Fishov I and Feingold M 2008 The shape of non-septated *E. coli* is asymmetric *Phys. Rev. E* **77** 061902
- [45] Gu M 2000 *Advanced Optical Imaging Theory* (Berlin: Springer)
- [46] Fu G, Huang T, Buss J, Coltharp C, Hensel Z and Xiao J 2010 *In vivo* structure of the *E. coli* FtsZ-ring revealed by photoactivated localization microscopy (PALM) *PLoS One* **5** e12680
- [47] Sun Q and Margolin W 1998 FtsZ Dynamics during the division cycle of live *Escherichia coli* cells *J. Bacteriol.* **180** 2050–6
- [48] Fischer-Friedrich E and Gov N S 2011 Modeling FtsZ ring formation in the bacterial cell—anisotropic aggregation via mutual interactions of polymer rods *Phys. Biol.* **8** 026007
- [49] Zhuo L, Trimble M J, Brun Y V and Jensen G J 2007 The structure of FtsZ filaments *in vivo* suggests a force-generating role in cell division *EMBO J.* **26** 4694–708
- [50] Chen Y and Erickson H P 2005 Rapid *in vitro* assembly dynamics and subunit turnover of FtsZ demonstrated by fluorescence resonance energy transfer *J. Biol. Chem.* **280** 22549–54
- [51] Wang X, Huang J, Mukherjee A, Cao C and Lutkenhaus J 1997 Analysis of the interaction of FtsZ with itself, GTP, and FtsA *J. Bacteriol.* **179** 5551–9
- [52] Rueda S, Vicente M and Mingorance J 2003 Concentration and assembly of the division ring proteins FtsZ, FtsA, and ZipA during the *Escherichia coli* cell cycle *J. Bacteriol.* **185** 3344–51
- [53] Gueiros-Filho F J and Losick R 2002 A widely conserved bacterial cell division protein that promotes assembly of the tubulin-like protein FtsZ *Genes Dev.* **16** 2544–56